



Stability Analysis and Support Control for a Jointed Soft Rock Roadway Considering Different Lateral Stresses

Shaohua Du · Diyuan Li · Weijian Yu · Jian Zhang · Fangfang Liu

Received: 6 April 2019 / Accepted: 15 July 2019 / Published online: 25 July 2019
© Springer Nature Switzerland AG 2019

Abstract The stability of coal mine roadways in jointed soft rock masses is an important issue for safe and efficient mining production in underground mines. Taking a main haulageway of a coal mine in Guizhou Province in China as the research background, the instability failure caused by large deformation of a roadway in a cracked rock mass was analysed, and its support control measures were put forward. First, the stability of the surrounding rock was evaluated by field investigation on the failure characteristics and statistics for the development of joints and fissures in the surrounding rock. Second, the corresponding numerical model was established by using FLAC^{3D} software, and the influence of the lateral pressure coefficient λ on the plastic zone and principal stress were analysed quantitatively. In addition, the evolution process of the

plastic zone over time was summarized. Furthermore, the key points of the reinforcement plan and support parameter design were provided on the basis of the technical approach for deformation control of the surrounding rock of the roadway. The original supporting scheme was optimized step by step, and the combined supporting scheme with “short bolt, long anchor cable and two-step grouting shell” serving as the main concept was put forward. Finally, the results of numerical calculation and field practice showed that the optimized scheme could effectively restrain the local deformation in the plastic zone of the surrounding rock of the roadway. The overall deformation was in a controllable range. In addition, the reinforced anchor cable was anchored to the deep part of the surrounding rock, ensuring the safety and stability of the roadway.

S. Du · D. Li (✉)
School of Resources and Safety Engineering, Central South University, Changsha 410083, Hunan Province, China
e-mail: diyuan.li@csu.edu.cn

S. Du
Work Safety Key Lab on Prevention and Control of Gas and Roof Disasters for Southern Coal Mines, Hunan University of Science and Technology,
Xiangtan 411201, Hunan Province, China

W. Yu · J. Zhang · F. Liu
School of Resources and Environment and Safety Engineering, Hunan University of Science and Technology, Xiangtan 411201, Hunan Province, China

Keywords Lateral pressure coefficient · Jointed soft rock · Plastic zone · Rock roadway · Stability analysis · Combined support

1 Introduction

Coal mines in Southern China are usually situated in a complex geological environment. With the features of a discontinuous geological structure and developed defects in the rock mass, the shape, orientation and size of the structure are determined by the

development degree, distribution density and mechanical properties of the fissure. These factors also control the stability and strength of the surrounding rock mass (Yuan et al. 2018a; Zhang et al. 2015; Yu and Liu 2018; Zhang et al. 2014; Zhao et al. 2018, 2019). For a rock mass roadway with a developed fracture, during the excavation and support control, the redistribution of the stress field and the local stress concentration around the surrounding rock results in a damage disturbance zone forming in shallow rock. The mechanical properties of the surrounding rock are further weakened and broken, showing complex features such as nonlinear large deformation and brittle-ductile transformation (Zhao et al. 2017; Li et al. 2015). According to field engineering practice (Jiao et al. 2013; Chen et al. 2018; Zheng et al. 2018), under various combined supports with ‘bolt + wire mesh + anchor cable (or U-shaped steel or grouting)’ as the primary support, the deformation of the roadway in cracked rock mass was seriously damaged, and the supporting structures often failed, in turn resulting in an increased amount of maintenance or repairs needed in the later period. As a result, the construction and operation costs of the project substantially exceeded the budgeted costs.

In view of the stability of the roadway under complex geological conditions, from different perspectives of mining, engineering geology, mechanics and other disciplines, Chinese and other scholars worldwide have made many beneficial explorations on the law of fracture expansion and evolution, the mechanical characteristics, the instability mechanism of the surrounding rock and the support theory of roadways (Zhao et al. 2016; Mao et al. 2011; Li et al. 2019). For example, in response to such challenges in roadways with high stress in deep underground engineering, Wang et al. (2018) analysed the main reasons leading to the support failure mechanisms of a roadway in the Zhaolou coal mine, a typical kilometre deep well, and put forward to a support system with square steel confined concrete (SQCC), which proved to be effective for surrounding rock control on the site; In the extended segment of the – 850 m main haulageway of Qujiang Mine, Wang analysed the development processes of the plastic zone in a soft rock roadway with high geo-stresses by the theoretical analysis method, numerical simulation method and other techniques and presented the comprehensive support method with “bolt wire cable and shotcrete +

floor anchor cable + local anchor cable or grouting reinforce”, which was successfully applied to the roadway (Wang et al. 2015); Yang described a case study of the failure mechanisms and stability control technology of a deep roadway with a soft rock mass in the Xin’an coal mine in Gansu Province, established the numerical model of a ventilation roadway by the UEDC software to study the failure process of a roadway under unsupported and primary support conditions and illustrated clearly the deformation, and finally proposed a new “bolt-cable-mesh-shotcrete + shell” combined support (Yang et al. 2017).

In previous studies, the research focused on the ideal surrounding rock mass. However, there are few reports on the stability analysis and support control for a roadway in a cracked rock mass. Therefore, addressing the problems of serious damage and difficult support for a roadway in a cracked rock mass, a + 600 m main haulageway of a coal mine in Guizhou Province was selected as the research object in this paper. The stability of the surrounding rock of the roadway under the lateral pressure coefficient is discussed by a combination of site investigation, joint statistics and numerical calculation. The reinforcement scope and key parts were determined, and the supporting scheme was optimized step by step. A targeted, economic and reasonable support scheme and control countermeasures were proposed and verified by numerical calculation and field practice. Therefore, this study possesses great practical value for studying the prevention and maintenance of engineering disasters caused by a cracked rock mass.

2 Engineering Background

2.1 Engineering Geology

A coal mine is located in Bijie, Guizhou Province, China, and the specific geographical location is shown in Fig. 1. The mining area can be classified mainly as a carbonate karst landform. The overall trend of the mountain is northeast, and the terrain is high in the south and low in the north. The maximum elevation is 1092.1 m, and the minimum elevation is approximately 760 m. The region is a subtropical monsoon climate that is characterized by much rain, a moist, temperate climate, warm conditions in the winter, and cool conditions in summer. The overall structure in the



Fig. 1 Geographical position of the coal mine

area is monoclinic and relatively simple. The annual design production capacity is 0.6 Mt, and the service life is 38.5 years. There are mainly five coal seams in the minefield that are mined, and they are numbered #2, #3, #4, #4-1 #5 and #7 from top to bottom. Moreover, the coal seams belong to simple structures and are relatively stable, with medium coal quality. In addition, the dip angle is relatively low, on average 8° .

With the buried depth of 300 m, a + 600 m main haulageway of the coal mine, located at the + 600 m level and contacting the + 600 m level yard, is mainly used for transportation in mining area I and lies in the siliceous limestone between the No. 4 coal seam and the No. 5 coal seam, whose overall length is 1651.2 m

(among which the + 600 m level yard is approximately 194.2 m). In particular, the roadway lies 11.8 m from the No. 4-1 coal seam and 22.85 m from the No. 4 coal seam. The roadway floor lies 10–12 m from the No. 5 coal seam. The roof and two sides of the roadway are arranged in the middle and lower part of the siliceous limestone layer, and the roadway floor is siltstone, which is obviously affected by the horizontal tectonic stress. Figures 2 and 3 show the layout of the + 600 m main haulageway and the comprehensive rock stratum histogram, respectively (Du et al. 2019).

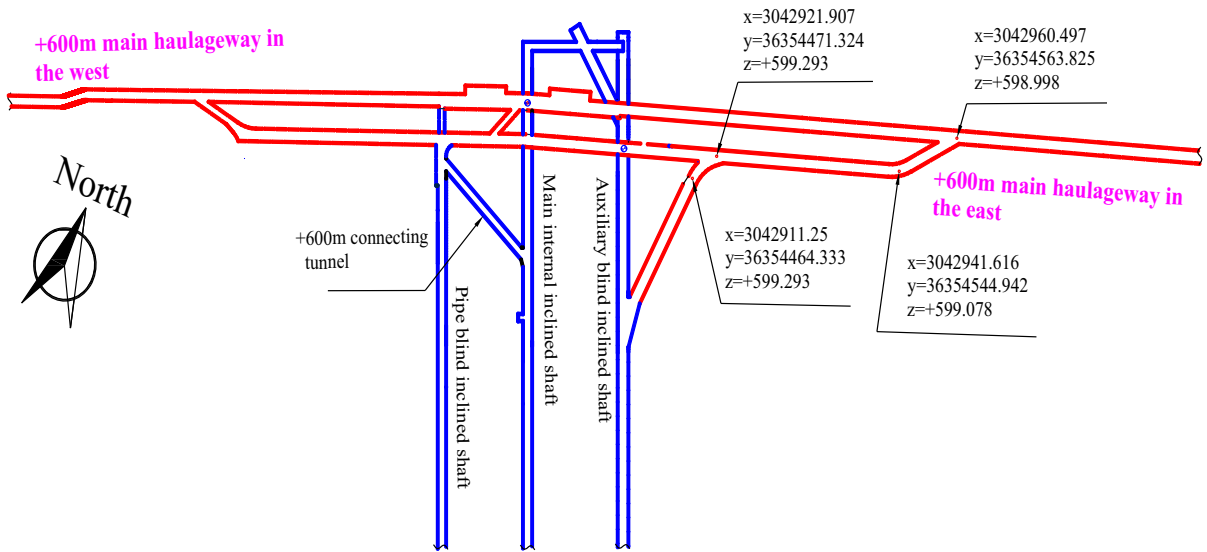


Fig. 2 The layout of the + 600 m main haulageway

Lithology	Thickness /m	Lithologic character	Diagrammatic cross-section
Coal seam #4	2.16	Black, metallic lustre, shell-like fracture, dense structure, layered construction.	
Fine sandstone, Clay rock	6.40	Grey, dark grey thin to medium thick layered fine sandstone, clay rock with a small amount of silt clay.	
Coal seam #4-1	2.49	Black or black-brown, metallic lustre, heterogeneous fracture, dense structure, layered construction, not to be adopted.	
Siltstone	8.60	Grey thin to medium and thick layered, including coal seam 1 with a thickness of 0.10-0.62 m in the local area.	
Siliceous	10.70	Dark gray, grey-black medium thick layered siliceous limestone, hard, dense, containing carpal fossils and fragments.	
Fine sandstone, Clay rock	7.80	Grey, dark grey thin to medium thick layered fine sandstone, clay rock with a small amount of silt clay.	
Coal seam #5	1.46	Black, metallic lustre, shell-like and heterogeneous fracture, complex structure.	
Fine sandstone, Clay rock	10.39	Grey, dark gray thin to medium thick layered fine sandstone, clay rock with a small amount of silt clay.	

Fig. 3 The comprehensive rock stratum histogram

2.2 Original Support and Deformation Failure Characteristics of the Roadway

In the + 600 m main haulageway, the area of the cross section is 16.75 m²; and the area of the net cross section is 15.71 m². As a support structure, the bolt-mesh-sprutting supporting technique was used in the section through the application of a high-strength resin screw-thread steel bolt of $\Phi 20 \text{ mm} \times 2000 \text{ mm}$ and a row and line spacing of $800 \times 800 \text{ mm}$, wire mesh with $\Phi 6.5 \text{ mm} - 100 \text{ mm} \times 100 \text{ mm}$, and C20 concrete with a thickness of 120 mm. The specific support form is shown in Fig. 4.

Through field investigation and mine pressure monitoring, the deformation and failure of the + 600 m main haulageway mainly manifested as the settlement of the roof being larger; the two shoulder parts were seriously broken, longitudinal cracks appeared, and the floor exhibited serious floor heave of greater than 300 mm. Additionally, the surrounding rock converged obviously, and the reduction of the cross-sectional area was over 40%, forming asymmetric deformation. Figure 5 shows the deformation and failure of the roadway in the field.

2.3 Investigation and Statistics of Joint Fracture

According to the detailed observation line method, the developed joints of the surrounding rock at the + 600 m main haulageway were measured by compass. The geometric parameters of 123 joints were obtained, and some of the results are shown in Table 1.

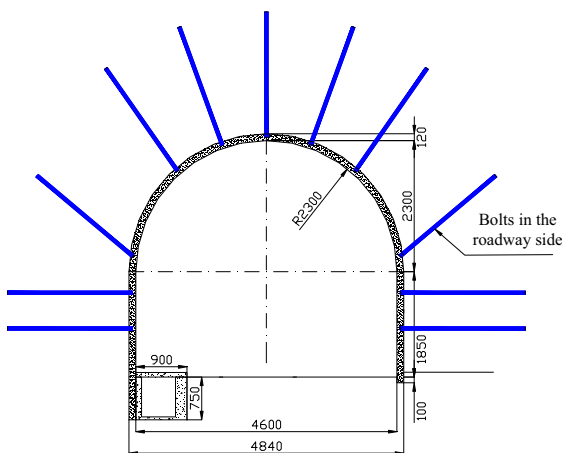


Fig. 4 Original support scheme

Then, the DIPS software was adopted to generate the density map of the pole projection, and the dominant orientation and the variation range of the occurrence of each group of joints were determined. The dominant joint group, its inclination and inclination angle, and the number of joints are shown in Fig. 6.

It can be found from the joint statistical dates that the spacing between the structural planes of the surrounding rock is 0.05–0.3 m, the number of volume joints J_v is 5–30/m³, with an average of 25/m³. The maximum spacing of joints is 30 cm, and the minimum spacing is less than 1 cm. On the other hand, as shown in Fig. 6, the joint cracks of the surrounding rock are relatively scattered, there is a group of jointed dominant planes that are mainly in the northeast and southwest, there tend to be more joints in the northwest direction, and the dip angle is concentrated at 60°–80°. Therefore, the joint fissure spacing of the surrounding rock is small and relatively developed, which is a fragmented structure type. Therefore, the integrity of the overall surrounding rock in the + 600 m main haulageway is poor.

3 Evolution Law for the Deformation and Fracture of the Jointed Soft Rock Roadway

Based on the abovementioned investigation of the roadway in the cracked rock mass and the statistical results for the joint fractures (Ma et al. 2018; Wang et al. 2019), the finite difference program Flac^{3D} software was used for numerical calculation in this section so that the influence of lateral pressure coefficient λ on the deformation and fracture of the roadway in cracked rock mass could be visually reflected.

3.1 Random Joint Model Establishment and Monitoring Point Placement

A semi-circular arch model roadway was built with an overall size of 50 m × 50 m × 20 m (X × Z × Y), totaling 209,450 zones. During the excavation process, displacement boundary constraints were imposed on each surface of the model, in which the floor was fully constrained and the sides horizontally constrained, and the vertical stress was 7.5 MPa on the roof surface. The Mohr–Coulomb model was used in the calculation model, and the adopted failure criterion

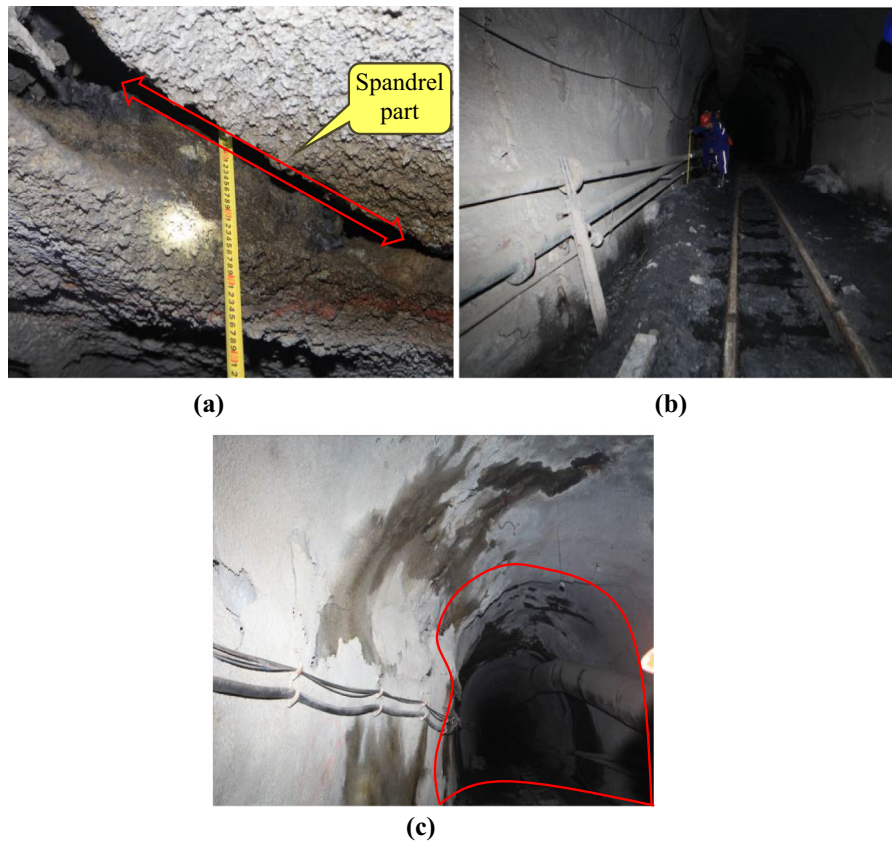
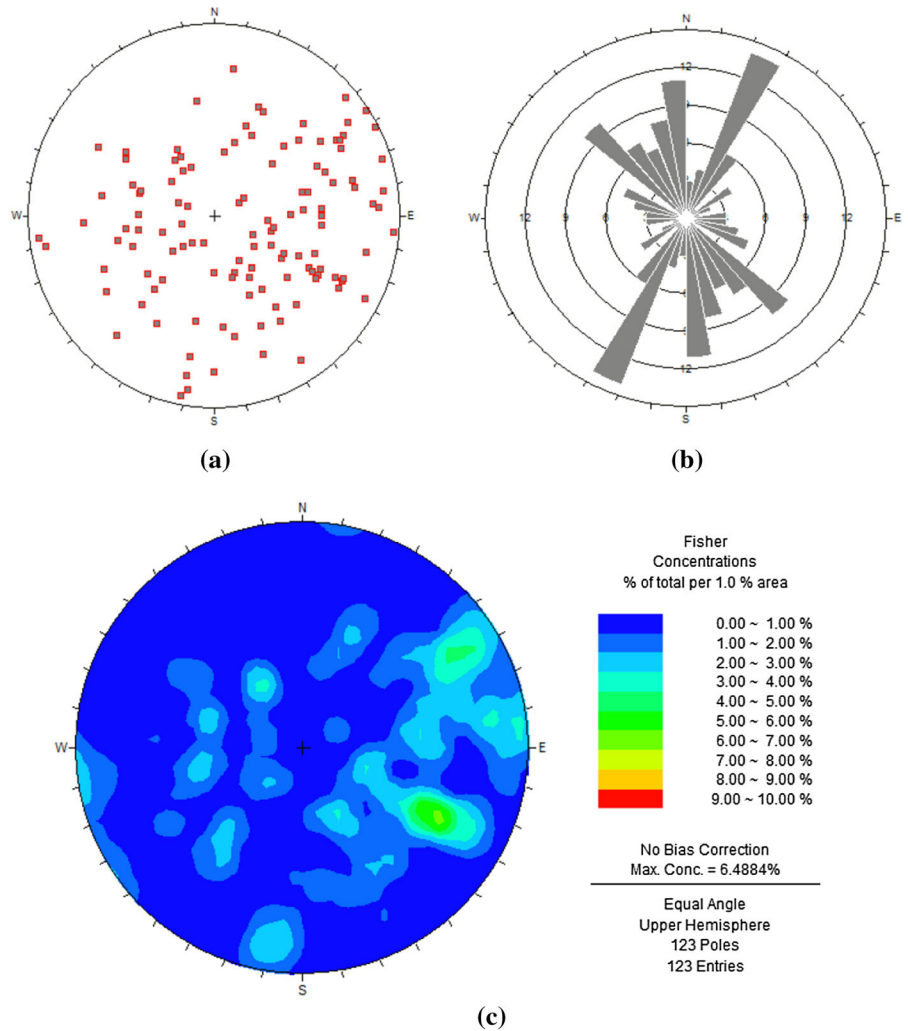


Fig. 5 Deformation and failure of a roadway in the field. **a** The broken shoulder parts, **b** floor heave and **c** convergent deformation of the cross-sectional area

Table 1 + 600 m Surrounding rock joint survey (part)

Basal spur (m)	Occurrence (°)		Type	Persistence length (cm)	Roughness type	Open type	Filling and type	Weathering degree
	Dip angle	Tendency						
0.71	38	116	4A	123	III	Heal		Slight
1.05	45	89	4A	145	III	Heal		Medium
1.27	60	90	4A	121	III	Close	Some clay	Higher
1.44	60	95	4A	155	IX	Close		Slight
1.60	75	116	4A	128	III	Close		Medium
1.81	46	118	4A	143	VIII	Open		Higher
2.19	62	351	4A	121	VII	Close		Medium
2.54	75	119	4A	117	III	Open		Medium
2.89	60	305	4A	125	II	Open	Some talc	Medium
3.46	75	8	4A	109	II	Open		Medium
3.89	86	49	4A	107	III	Open		Medium
4.26	89	62	4A	113	II	Open		Higher
4.89	88	95	4A	106	III	Open	Some clay	Medium

Fig. 6 Joints of surrounding rock of the roadway. **a** Section Chi-Ping projection pole chart, **b** joint walk towards the rose chart, and **c** density chart of the jointed poles



was a composite Mohr–Coulomb criterion; in addition, six monitoring pints were arranged on the roof, right side and floor of the roadway (the monitoring pints in the roof, right side, floor were R1–R6, T1–T6, and S1–S6, respectively). The model and monitoring pint are shown in Fig. 7.

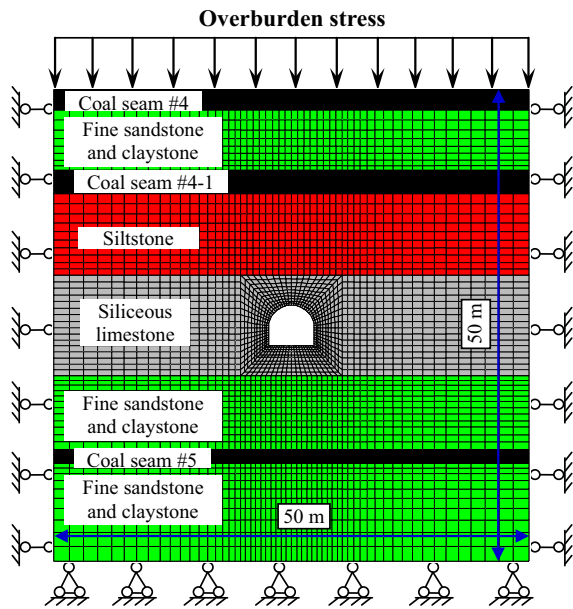
According to the geological rock stratum and joint fissure statistics and based on the geometric parameters, such as the dip angle and inclination of the joint advantage group, the random fracture network (DFN) module in the version software (Guo et al. 2011), as shown in Fig. 8. In this coordinate system, the Z direction is the tunnel excavation direction, the Y direction is the gravity direction, and the mechanical

parameters of the surrounding rock of the roadway are selected as shown in Table 2.

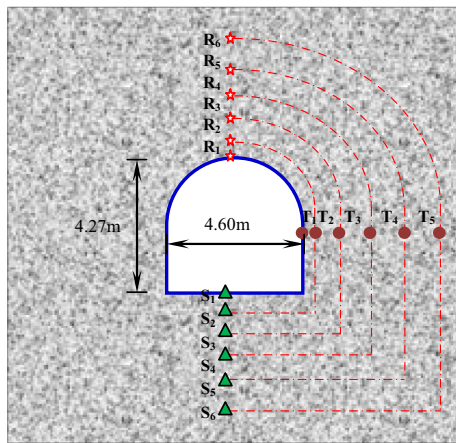
3.2 Influence of the Lateral Pressure Coefficient on the Principal Stress of the Surrounding Rock of the Roadway

1. Under the condition of different lateral pressure coefficients λ , the relationship curves between the maximum principal stress σ_1 (and the minimum principal stress σ_3) in the roof of the roadway and the distance from the free surface are shown in Fig. 9a, b, respectively.

As shown in Fig. 9, under different lateral pressure coefficients, the principal stresses σ_1 and σ_3 of the rock



(a)



(b)

Fig. 7 The model and monitoring points. **a** Boundary conditions of the calculation model and **b** the layout of the monitoring points

mass in the roof increase with increasing distance from the free surface. However, there is little difference for the corresponding principal stresses σ_1 and σ_3 in the shallow of the roof. In the deep rock mass, the higher the lateral pressure coefficient, the larger the principal stresses σ_1 and σ_3 , and the larger is the deviatoric stress ($\sigma_1 - \sigma_3$), which is extremely unfavourable for the stability of the surrounding rock. This finding indicates that the lateral pressure coefficient is sensitive to the principal stress of the rock mass in the roof, and the

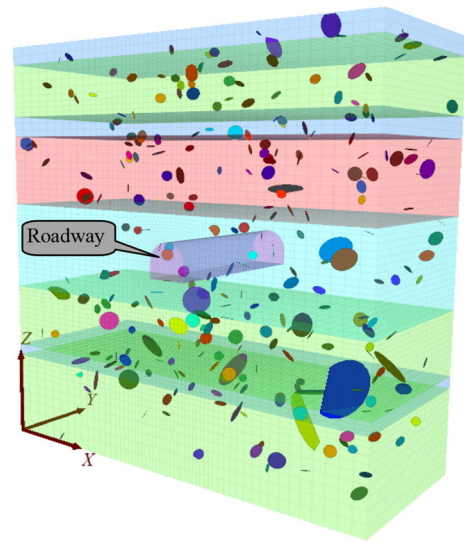


Fig. 8 Joint fissure model

release and transfer of the high stress in the deep rock mass should be considered.

2. Under the condition of different lateral pressure coefficients λ , the relationship curves on the right side of the roadway are shown in Fig. 10a, b.

Figure 10 shows that the maximum principal stress σ_1 increases with increasing distance from the free surface when the lateral pressure coefficient $\lambda \leq 1.2$, and the value is first linear and then decreases, but the influence of lateral pressure coefficient on the maximum principal stress σ_1 is small. When the lateral pressure coefficient $\lambda > 1.2$, the maximum principal stress σ_1 increases with the distance from the free surface, the effect on the maximum principal stress σ_1 is significant, and the discrimination degree is large after the depth of rock mass exceeds 3.5 m. Therefore, the lateral pressure coefficient λ has less effect on the rock mass on the two sides of the roadway, and the high lateral pressure coefficient does not necessarily cause more damage to the rock mass.

3. Under the condition of different lateral pressure coefficients λ , the relationship curves for the floor of the roadway are shown in Fig. 11a, b.

According to what is shown in Fig. 11, the conclusion is drawn that the principal stresses σ_1 and σ_3 under different lateral pressure coefficients λ slowly increase with increasing distance from the free surface, and the stress values are roughly equal. After the distance

Table 2 Calculation mechanics parameters of the rock strata

Surrounding rock	Unit weight ($\gamma/\text{g cm}^{-3}$)	Uniaxial compressive strength (R/MPa)	Uniaxial tensile strength (R_t/MPa)	Cohesive force (C/MPa)	Inner friction angle ($\Phi/^\circ$)	Elasticity modulus (E/GPa)	Poisson ratio (μ)
Fine sandstone, clay rock	2.65	12.09	0.47	3.34	35	1.26	0.34
Siliceous limestone	2.32	17.02	0.64	3.32	30	4.38	0.32
Siltstone	2.65	8.28	0.31	4.25	31	11.65	0.21
Coal seam #4, #4-1 and #5	1.6	12	1.43	1.50	33	0.45	0.42

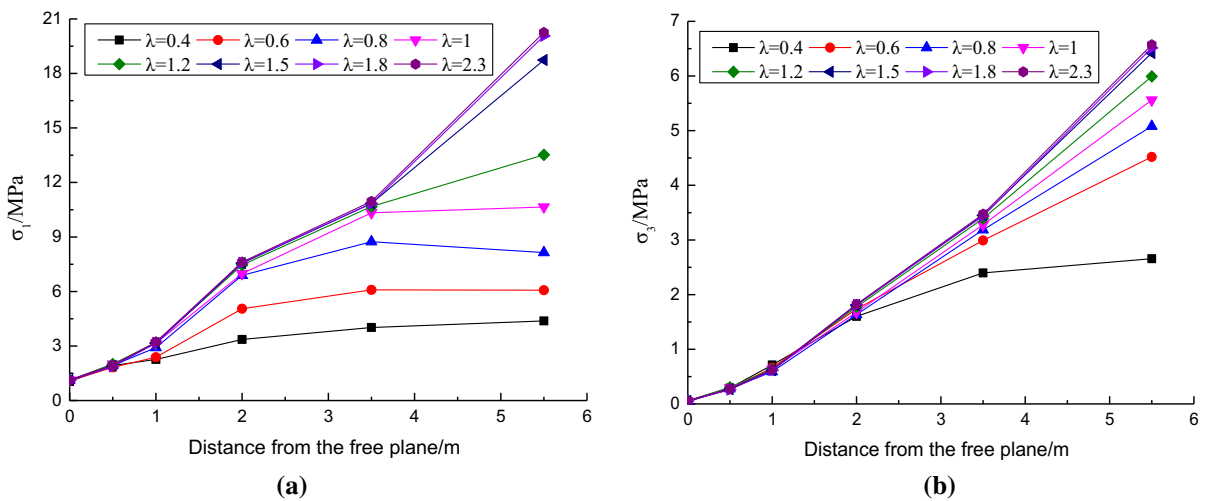


Fig. 9 The stresses of monitoring pints in the roof of roadway. **a** The maximum principal stress- σ_1 and **b** the minimum principal stress- σ_3

exceeds 2 m, the growth rate of the principal stresses σ_1 and σ_3 is accelerated, the deviatoric stress ($\sigma_1 - \sigma_3$) is sharply increased, and the stress concentration is concentrated in the floor of the roadway. Moreover, the stress at each point in the floor is clearly distinguished when the lateral pressure coefficient $\lambda < 1$ and the sensitivity is higher than that when $\lambda > 1$. This result indicates that the stress of the surrounding rock in the shallow part of the floor has transferred to the deep part, and the lateral pressure coefficient mainly causes the high stress concentration area in the deep part of the floor. Additionally, the higher the lateral pressure coefficient, the more concentrated the stress is, and the easier it is to exacerbate the occurrence of the floor heave.

3.3 Distribution of the Plastic Zone Considering Different Lateral Pressure Coefficients

As shown in Fig. 12, it can be seen that, when the lateral pressure coefficient $\lambda \leq 1.0$, the plastic zone of the roadway mainly expands from the side to the roof with increasing lateral pressure coefficient, and the overall shape of the plastic zone is transformed from a butterfly to a rounded rectangle, to an ellipse, and then to a circle, and the maximum normal distance L between the location of the plastic zone and the free side of the roadway, increases with the decrease in the lateral pressure coefficient. When the lateral pressure coefficient $\lambda > 1.0$, the plastic zone first expands from the roof to the two sides of the roadway; the change of the plastic zone shape is just the

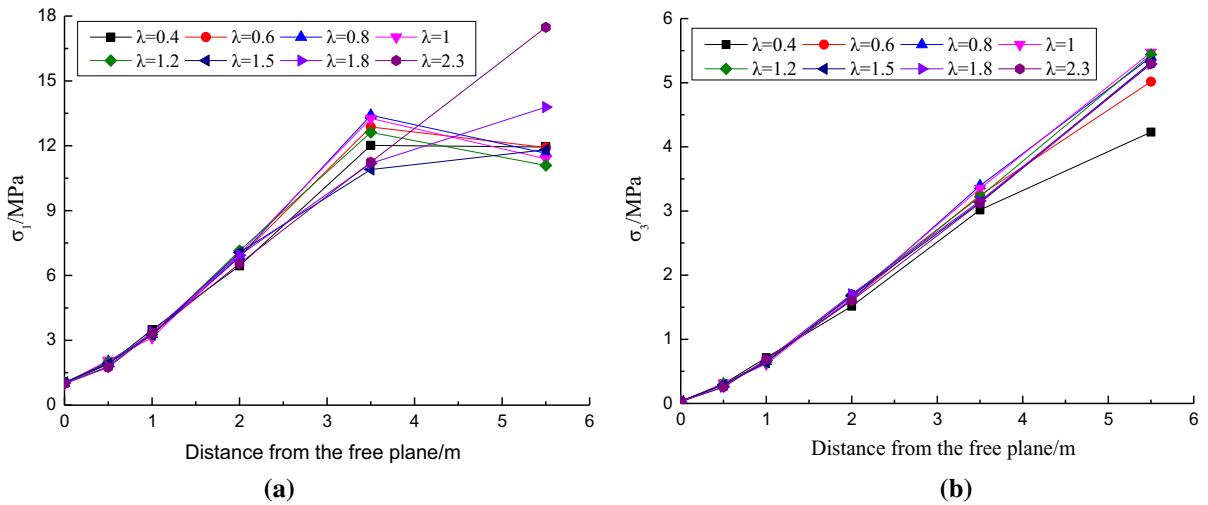


Fig. 10 The stresses of the monitoring points on the right side of the roadway. **a** The maximum principal stress- σ_1 and **b** the minimum principal stress- σ_3

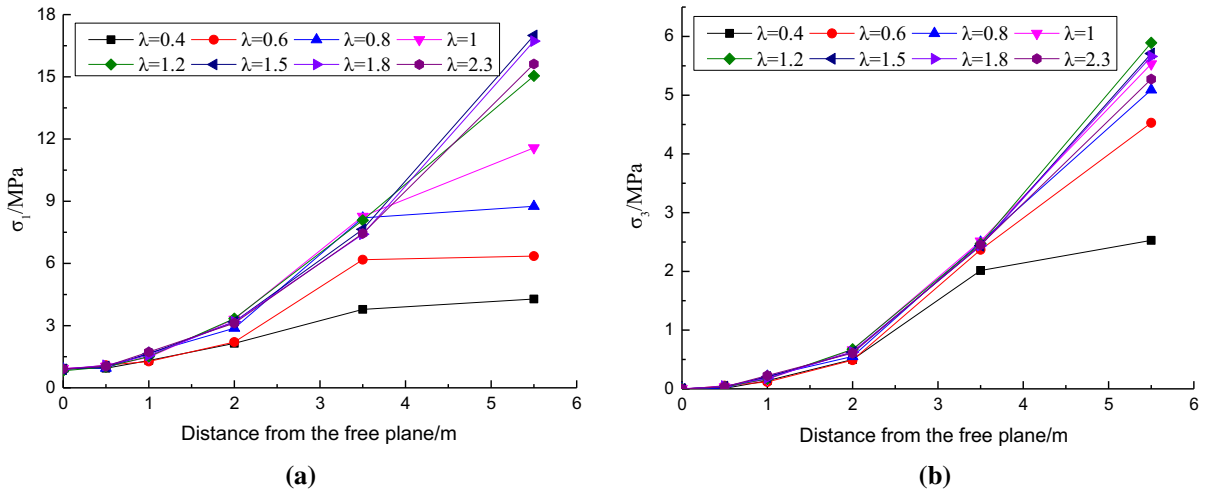


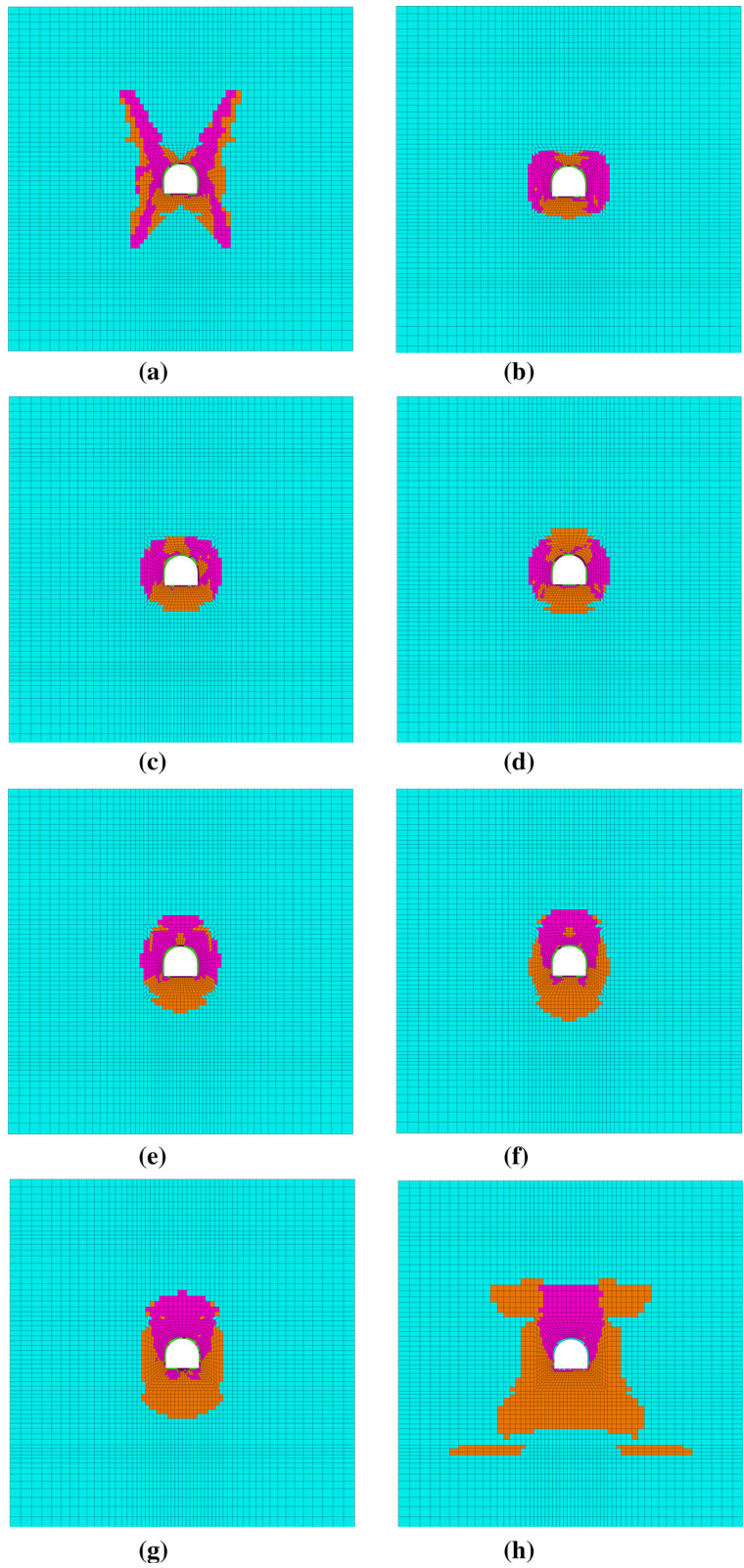
Fig. 11 The stresses of monitoring points at the roof. **a** The maximum principal stress- σ_1 and **b** the minimum principal stress- σ_3

opposite, but the overall range of the plastic zone is larger. In summary, the plastic zone expansion morphology and its maximum radius are sensitive to changes in the lateral pressure coefficient.

At the same time, the initial formation position, development process and final shape of the plastic zone under different lateral pressure coefficients λ were observed, and it was found that the change in the maximum value L of the plastic zone goes through five stages, including local distortion, uneven expansion and hazardous expansion (Wang et al. 2015; Li et al. 2017; Yuan et al. 2018b), as shown in Fig. 13. The details are as follows: ① Plastic point stage I: After the

roadway was excavated, the plastic point first appeared at the four corners of the roof and floor (point A); ② Plastic ring stage II: each plastic point gradually penetrated into a circle, would be linked into a ring, and moved into a local ring with the iteration time t , which was more evenly distributed in the shallow part of the surrounding rock (point B); ③ Local distortion stage III: local distortion began in the high stress concentration of the roadway, but the duration was short; ④ No uniform expansion stage IV: Local distortion led to uneven expansion (point C): With time advancement, the uneven spread and differentiation became intense, and the irregular shape

Fig. 12 Extension of the plastic zone considering different lateral pressure coefficients. **a** $\lambda = 0.4$, **b** $\lambda = 0.6$, **c** $\lambda = 0.8$, **d** $\lambda = 1.0$, **e** $\lambda = 1.2$, **f** $\lambda = 1.5$, **g** $\lambda = 1.8$ and **h** $\lambda = 2.3$



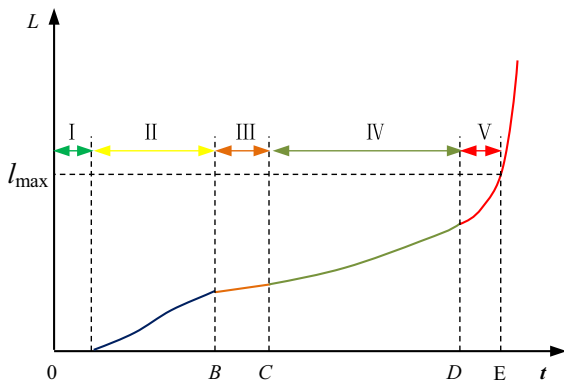


Fig. 13 Hazardous expansion of the plastic zone

of the plastic zone was formed, resulting in large deformation of the roadway; ⑤ Hazardous expansion of the large plastic zone, which would continue to accelerate and expand to reach the maximum value L_{max} near the unstable state (point E).

4 Effective Ways of Support Control for the Jointed Soft Rock Roadway

As mentioned above, the plastic zone of the surrounding rock of the roadway is always accompanied by stress. Improving the overall mechanical properties of the surrounding rock by inhibiting the malignant expansion of the plastic zone provides an important basis for the reinforcement scheme and design of the supporting parameters to promote the stability control of the roadway.

4.1 Factors Affecting the Stability

Classic ideal elastic–plastic theory was further improved by H. Kastner on the basis of Fenner’s research, and the characteristic curve equation of surrounding rock in an underground chamber was obtained, namely, the famous Kastner formula (Cheng 2012).

$$R = a \left[\frac{(p_0 + c \cdot \cot \varphi)(l \sin \varphi)^{\frac{1-\sin \varphi}{2 \sin \varphi}}}{p_i + c \cdot \cot \varphi} \right] \quad (1)$$

$$u_0 = \frac{\sin \varphi}{2G \cdot a} \cdot (p_i + c \cdot \cot \varphi) \cdot R^2 \quad (2)$$

where R is the radius of the plastic zone of the surrounding rock of the roadway, m; a is the radius of the roadway section, m; p_0 is the original rock stress, MPa; p_i is the support resistance, MPa; c is the cohesion, MPa; φ is the internal friction angle, ($^\circ$); u_0 is the displacement around the roadway, m; and G is the shear modulus, GPa.

From Eqs. (1) and (2), it can be seen that the main factors affecting the stability of the surrounding rock of the roadway include the stress of the surrounding rock p_0 , the mechanical properties of the surrounding rock (c, φ, G), the support resistance (p_i), and the form and size of the roadway section. In other words, controlling the stress of the surrounding rock, enhancing the integral strength of the surrounding rock, and increasing the support strength could effectively improve the stability of the surrounding rock of the roadway.

4.2 Technical Way to Control the Stability

According to the law of lateral pressure coefficient on the deformation and fracture of a roadway in cracked rock and the factors to control the stability of surrounding rock of the roadway, three basic technical ways to control the these parameters under this condition were proposed: grouting reinforcement, the support system of high strength anchor and the strengthened support in key parts of roadway. The details are as follows:

1. Grouting reinforcement. Grouting in the surrounding rock can alleviate the high stress concentration, reduce the fractured area, and further cut off the water source, which improves the initial anchoring force and anchoring force of the supporting structure.
2. Improving the initial support strength. Strengthening the surrounding rock by improving the initial strength of bolts is achieved by forming a high-strength internal load-bearing structure as early as possible and narrowing the area of the fracture zone in the shallow part of the surrounding rock;
3. Strengthening the support in key parts of the surrounding rock of the roadway. The key to partial reinforcement is to control the malignant expansion of the plastic zone; for example, stress concentrations easily occur in the roadway

spandrel and two corners of the floor. These sensitive parts can be controlled by means of high-resistance anchors or long anchors.

4.3 Support Scheme Design and Numerical Simulation

Based on the above description, combined with the geological conditions, the parameters of the original support scheme are gradually optimized in a step-by-step manner, and the following four support schemes are considered for numerical simulation analysis in order to obtain the best support scheme suitable for the actual situation. The design schemes are as follows:

Original scheme: bolt, metal mesh, and concrete shotcrete, that is, the bolt-mesh-sprutting support;

Scheme 1: Based on the original support scheme, optimizing the parameters of bolts, including the length, pre-tightening force, and row and line spacing, mainly serving the primary support.

Scheme 2: On the basis of Scheme 1, grouting and strengthening the key parts of the roadway.

Scheme 3: On the basis of Scheme 2, long anchor cable and bolts are added to the sensitive parts of the roadway in order to further reinforce and strengthen the surrounding rock.

According to the above ideas, a three-dimensional numerical model was established by the software Flac^{3D}. The stress field, displacement field and morphological characteristics of the plastic zone of the roadway under each scheme were obtained through iterative calculation, and the mechanical parameters of each rock layer used in the calculation are listed in Table 2. Figure 14 shows the distribution of each support scheme and its plastic zone, and Fig. 15 shows the final convergence values of the monitoring points.

As shown in Figs. 14 and 15, compared with the results of the original scheme, although the support parameter was optimized and the bolts were added to the floor, the range of the plastic zone was not significantly reduced, and the convergence displacement of the surrounding rock was only partially weakened. In a comparison with the results of scheme 1, the range of the plastic zone decreased obviously, and the maximum convergence displacement of the surrounding rock was reduced by 20.8%

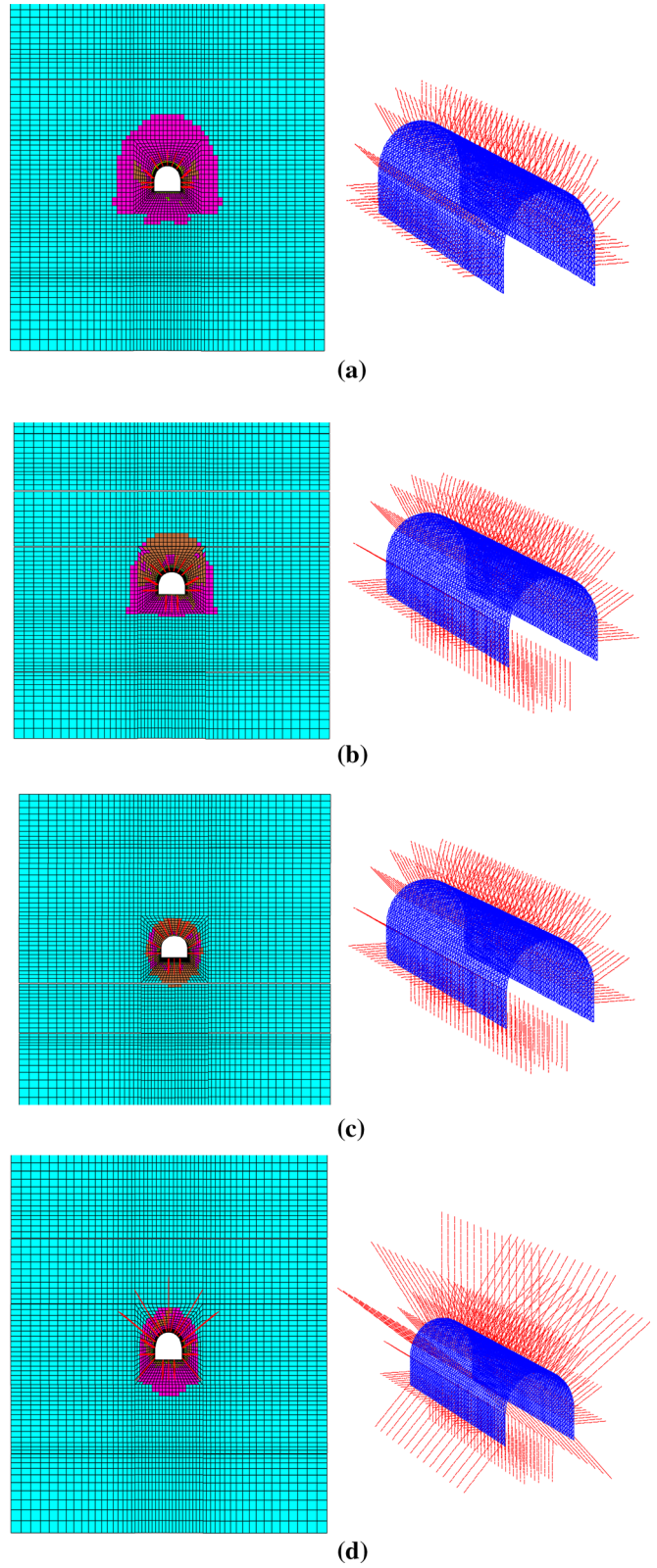
and 36.3%, respectively, but the supporting structure was still in the plastic zone, and the convergence displacement rock was also larger. After the long anchor cable in the roof and spandrel and bolts were installed in two corners of the floor on the basis of scheme 2, it was found that the end of the long anchor cable was far beyond the plastic zone and was anchored to the deep intact rock mass, and the convergence deformation of the surrounding rock was essentially controlled. In addition, the maximum convergence displacement of the surrounding rock was reduced by 72.2% and 77.1% compared with the results of the original scheme, and the final convergence displacement between the roof and floor and the two sides of the roadway were 180.9 mm and 171.1 mm, respectively. In conclusion, scheme 3 can better restrain the deformation and destruction of such roadways and is conducive to maintaining its long-term stability.

5 Proposed Support Scheme and Support Effect

To verify the effectiveness and feasibility of the proposed optimal support scheme (Scheme 3), the combined supporting scheme with “short bolt, long anchor cable and two-step grouting shell” as the main concept was adopted in the field. Figure 16 shows the specific support parameters for the +600 m main haulageway in the A coal mine as follows:

1. Bolts: high-strength, high-prestressed resin screw-thread steel bolts with dimensions of $\Phi 20$ mm \times 2400 mm, a row and line spacing of 700 \times 1400 mm, an anchor length of 1200 mm, a pre-tightening force of 15 kN, and the limit anchorage force of no less than 235.5 kN.
2. Anchor cable: The anchor cable is composed of 19 strands with high strength and low relaxation, with a diameter of 17.8 mm and a row and line spacing of 1400 \times 1400 mm. The lengths of the anchor cable in the roof and two corners of the floor are 7000 and 4000 mm, respectively. The anchor cable in two corners of the floor is at an angle of 45 degrees to the horizontal plane, and the resin coils are anchored with an anchoring length of 1500 m. And what's more, a pre-tightening force is 75 kN, and the limit anchorage force is no less than 320 kN.

Fig. 14 Each supporting scheme and its plastic zone form. **a** Original scheme, **b** scheme 1, **c** scheme 2 and **d** scheme 3



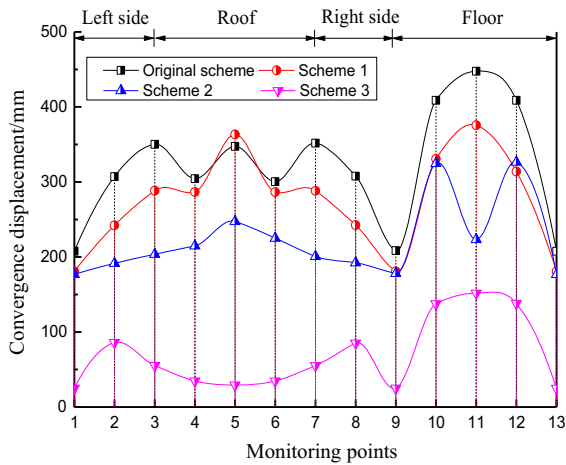


Fig. 15 Displacement of each monitoring point

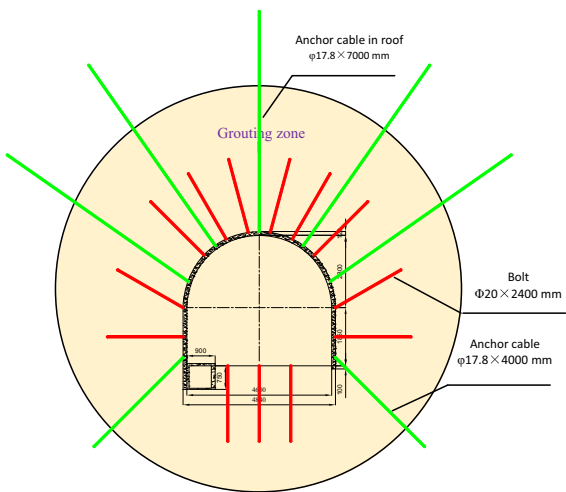


Fig. 16 Support form in the field

3. Grouting: four grouting holes are arranged in the whole section, the depth of grouting is 5 m, the grouting material is high-water-content quick setting material, and the water-cement ratio is 1.2:1.

Figure 17 shows the monitoring results of the surrounding rock of the roadway after the optimal support scheme was implemented. From the point of view of convergence displacement, the deformation of the surrounding rock of the roadway changed relatively fast in the early stage, was in a slow deformation stage in the later stage, and finally tended to a stable state. The final convergence displacements of the two sides and the roof and floor of the roadway

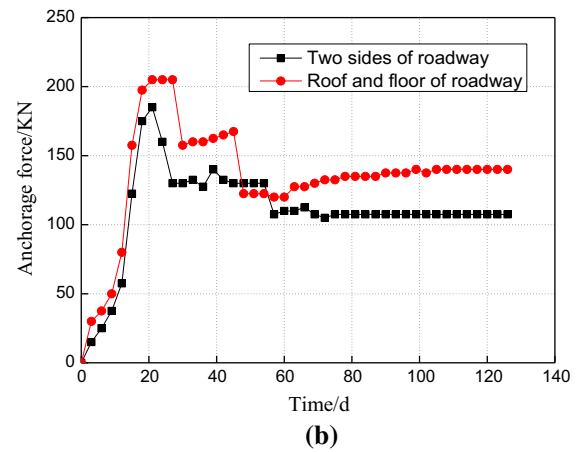
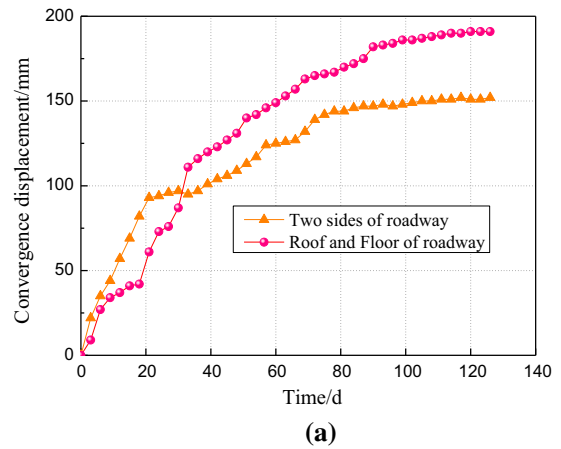


Fig. 17 Monitoring curve of the surrounding rock of the roadway under the optimization scheme. **a** The convergence displacement curve of the roadway and **b** the anchorage force curve of the supporting structure

were 152 mm and 191 mm, respectively. According to the anchorage force condition of the supporting structure, the value gradually increased during the first 20 days; the growth rate was very fast, and then the value began to decrease, but it tended to be stable and ultimately maintained a higher level. Therefore, the proposed combined support technology with a “step-by-step strengthening supporting effect to achieve internal and external load-bearing structure” as the core concept can meet the safety requirements of roadway production. The support effects on the field are shown in Fig. 18.



Fig. 18 Support effects in the field. **a** Section 1 and **b** section 2

6 Conclusions

1. Through field investigation and joint statistics, the deformation and failure of the surrounding rock in the + 600 m main haulageway was serious, the surrounding rock converged obviously, and the reduction of the cross-sectional area was over 40%. The joint fissure spacing in the surrounding rock was small and relatively developed, and the integrity of the overall surrounding rock was poor.
2. With increasing lateral pressure coefficient λ , the larger the deviatoric stress ($\sigma_1 - \sigma_3$) in the rock mass, the more likely a stress concentration arises in the deep rock mass, but this stress concentration has less influence on the rock mass on the two sides of roadway. For the shape expansion of the plastic zone, the more the lateral pressure coefficient deviates from 1, the more easily the butterfly shaped plastic zone is formed in the four corners of the roadway, where the range is large. The shape expansion of the plastic zone is distinctly distinguished.
3. Based on three basic technical ways for supporting the jointed soft roadway, including grouting reinforcement, high-strength bolts, and strengthening support in the key parts, the parameters of the original support scheme were gradually optimized in a step-by-step manner, and a total of four support schemes were designed.
4. According to numerical calculations and field practice, under the designed supporting scheme with “short bolt, long anchor cable and two-step grouting shell” as the main concept, there appeared no distortion plastic zone in the

surrounding rock of the roadway, and the overall deformation was restrained in a controllable range, and the ends of anchor cables were anchored in the deep surrounding rock and maintained a higher level, thus ensuring the long-term safety of the roadway.

Acknowledgements The work was financially supported by the National Natural Science Foundation of China (No. 51474250), the Innovation-driven Program Project of Central South University (No. 2018CX020), the Fundamental Research Funds for the Central Universities of Central South University (No. 2017zzts165), and the Open Research Fund Program of Work Safety Key Lab on Prevention and Control of Gas and Roof Disasters for Southern Coal Mines (Hunan University of Science and Technology) (No. E21827).

References

- Chen S, Wu A, Wang Y, Chen X, Yan R, Ma H (2018) Study on repair control technology of soft surrounding rock roadway and its application. *Eng Fail Anal* 92:443–455
- Cheng YM (2012) Modified kastner formula for cylindrical cavity contraction in mohr-coulomb medium for circular tunnel in isotropic medium. *J Mech* 20:163–169
- Du S, Li D, Sun J (2019) Stability control and support optimization for a soft-rock roadway in dipping layered strata. *Geotech Geol Eng* 37(3):2189–2205
- Guo Y, Zhu W, Yu D, Li X (2011) Study of a high slope stability considering the stochastic distribution of rock joint set. *Appl Mech Mater* 90–93:786–790
- Jiao Y-Y, Song L, Wang X-Z, Coffi Adoko A (2013) Improvement of the U-shaped steel sets for supporting the roadways in loose thick coal seam. *Int J Rock Mech Min Sci* 60:19–25
- Li, X., K. Du & D. Li (2015) True triaxial strength and failure modes of cubic rock specimens with unloading the minor principal stress. *Rock Mech Rock Eng* 48:2185-2196

- Li C, Shi W, Feng R (2017) Elastic–plastic analysis of surrounding rock in deep roadway considering shear dilatancy property under non-uniform stress field. *J Eng Sci Technol Rev* 10(4):16–24
- Li D, Han Z, Sun X, Zhou T, Li X (2019) Dynamic mechanical properties and fracturing behavior of marble specimens containing single and double flaws in SHPB tests. *Rock Mech Rock Eng* 52(6):1623–1643
- Ma C, Yao W, Yao Y, Li J (2018) Simulating strength parameters and size effect of stochastic jointed rock mass using DEM method. *KSCE J Civ Eng* 22:4872–4881
- Mao D, Nilsen B, Lu M (2011) Analysis of loading effects on reinforced shotcrete ribs caused by weakness zone containing swelling clay. *Tunn Undergr Space Technol* 26:472–480
- Wang Q, Jiang B, Pan R, Li S-C, He M-C, Sun H-B, Qin Q, Yu H-C, Luan Y-C (2018) Failure mechanism of surrounding rock with high stress and confined concrete support system. *Int J Rock Mech Min Sci* 102:89–100
- Wang F, Cao P, Cao R-h, Xiong X-g, Hao J (2019) The influence of temperature and time on water–rock interactions based on the morphology of rock joint surfaces. *Bull Eng Geol Environ* 78(5):3385–3394
- Wang W, Guo G, Zhu Y, Yu W (2015) Malignant development process of plastic zone and control technology of high stress and soft rock roadway. *J China Coal Soc* 40(12):2747–2754
- Yang S-Q, Chen M, Jing H-W, Chen K-F, Meng B (2017) A case study on large deformation failure mechanism of deep soft rock roadway in Xin'An coal mine, China. *Eng Geol* 217:89–101
- Yu W, Liu F (2018) Stability of close chambers surrounding rock in deep and comprehensive control technology. *Adv Civ Eng* 2018:1–18
- Yuan H-h, Shan R-l, Su X-g (2018a) Deformation characteristics and stability control of a gateroad in fully mechanized mining with large mining height. *Arab J Geosci* 11:767
- Yuan Y, Wang W, Li S, Zhu Y (2018b) Failure mechanism for surrounding rock of deep circular roadway in coal mine based on mining-induced plastic zone. *Adv Civ Eng* 2018:1–14
- Zhang C, Yang ZX, Nguyen GD, Jardine RJ, Einav I (2014) Theoretical breakage mechanics and experimental assessment of stresses surrounding piles penetrating into dense silica sand. *Geotech Lett* 4:11–16
- Zhang Z, Bai J, Chen Y, Yan S (2015) An innovative approach for gob-side entry retaining in highly gassy fully-mechanized longwall top-coal caving. *Int J Rock Mech Min Sci* 80:1–11
- Zhao Y, Zhang L, Wang W, Pu C, Wan W, Tang J (2016) Cracking and stress–strain behavior of rock-like material containing two flaws under uniaxial compression. *Rock Mech Rock Eng* 49:2665–2687
- Zhao Y, Zhang L, Wang W, Tang J, Lin H, Wan W (2017) Transient pulse test and morphological analysis of single rock fractures. *Int J Rock Mech Min Sci* 91:139–154
- Zhao Y, Zhang L, Wang W, Wan W, Ma W (2018) Separation of elastoviscoplastic strains of rock and a nonlinear creep model. *Int J Geomech* 18:04017129
- Zhao Y, Wang Y, Wang W, Tang L, Liu Q, Cheng G (2019) Modeling of rheological fracture behavior of rock cracks subjected to hydraulic pressure and far field stresses. *Theor Appl Fract Mech* 101:59–66
- Zheng W, Zhao Y, Bu Q (2018) The coupled control of floor heave based on a composite structure consisting of bolts and concrete antiarches. *Math Probl Eng* 2018:1–14

Publisher's Note Springer Nature remains neutral with regard to jurisdictional claims in published maps and institutional affiliations.